Heat flow and mass diffusion in binary Lennard-Jones mixtures

Sten Sarman and Denis J. Evans
Research School of Chemistry, Australian National University, Canberra, Australian Capital Territory 2601, Australia
(Received 14 February 1991; revised manuscript received 24 October 1991)

We have applied the Evans-Cummings (EC) nonequilibrium molecular-dynamics (NEMD) heat-flow algorithm for liquid mixtures to an equimolar Lennard-Jones (LJ) mixture where the potential parameters and the state point have been chosen to model an argon-krypton mixture at its triple point. We have calculated the thermal conductivity and the Soret coefficient for one 108-particle system and one 1024-particle system. In order to check the results we have used the color conductivity algorithm to obtain the mutual diffusion and the Dufour coefficients. According to the Onsager reciprocity relations the Dufour and the Soret coefficients should be equal, and this has also been found to be the case within the statistical uncertainty. The thermal conductivity and the diffusion coefficient increase slightly with the system size, but the statistical error makes it impossible to discern any size dependence of the cross-coupling coefficients. We also computed the Soret coefficient for three hypothetical types of LJ mixtures. A consistency control was done by evaluating the Green-Kubo (GK) relations for the different transport coefficients by performing an equilibrium molecular-dynamics simulation. The GK thermal conductivity and the diffusion coefficient agree very well with the NEMD results but GK cross-coupling coefficients are very noisy and the error is probably about 15%. The EC algorithm is a NEMD algorithm that violates adiabatic incompressibility of phase space, but this does not cause any difficulties.

PACS number(s): 44.30.+v, 44.10.+i

I. INTRODUCTION

In a liquid mixture, a temperature gradient does not only give rise to a heat flow but also to chemical-potential gradients. These gradients induce mass currents of the various components in the mixture. This phenomenon is known as the Soret effect [1] and the cross-coupling coefficients relating the temperature gradients and the mass currents are known as Soret coefficients. Conversely, a chemical-potential gradient also causes heat flow, which is known as the Dufour effect with a corresponding Dufour cross-coupling coefficient. According to the Onsager reciprocity relations (ORR) the Dufour and the Soret coefficient should be equal. There have been various attempts to calculate these coefficients by applying molecular-dynamics (MD) methods. There are basically two categories of MD methods for computing transport coefficients, namely synthetic homogeneous nonequilibrium molecular-dynamics (NEMD) methods and equilibrium molecular-dynamics (EMD) methods. In the first case one couples the system to an external field and the transport coefficient is obtained in the limit of zero field. In the latter case the Green-Kubo (GK) relation for the transport coefficient in question is evaluated.

A successful effort to calculate cross-coupling coefficients was made by McGowan and Evans [2] in 1986. They devised a NEMD heat-flow algorithm for ideal mixtures, which will be referred to as the ME algorithm in the rest in this article, and they applied it to an equimolar Lennard-Jones (LJ) mixture where the different potential parameters and the state point were chosen to model an argon-krypton mixture at its triple point. Their results were confirmed by Paolini and Ciccotti [3], who used the same algorithm augmented with a subtraction noise-reduction method [4]. Apart from these two works most other attempts have been based on EMD evaluations of GK integrals. The first of these simulations tried to repeat the NEMD results [4,5], but later works have covered different systems like hard-sphere systems [6] and a wider range of LJ fluids [7–9].

The main drawback with the ME algorithm is that it is only strictly valid for ideal mixtures. In order to be able to calculate transport coefficients of more realistic mixtures a more general algorithm is required. A solution to this problem was suggested by Evans and Cummings (EC) [10]. They devised a completely general NEMD algorithm for heat flow in a mixture of simple fluids. Their algorithm makes it possible to unambiguously calculate both the thermal conductivity and the Soret coefficient. In this paper we will test this method for the same system as in Ref. [2] which is almost an ideal mixture, so we expect the results to be similar. In Sec. II we present the necessary theory, in Sec. III the results are presented, and finally in Sec. IV there is a conclusion.

II. THEORY

A. Macroscopic theory

In a two-component mixture the thermodynamic forces and fluxes are formally related by the following relation:

$$\begin{aligned} \langle \mathbf{J}_1 \rangle &= L_{11}\mathbf{X}_1 + L_{1Q}\mathbf{X}_Q \ , \\ \langle \mathbf{J}_Q \rangle &= L_{Q1}\mathbf{X}_1 + L_{QQ}\mathbf{X}_Q \ , \end{aligned} \tag{2.1}$$

where $\langle \mathbf{J}_1 \rangle$ is the macroscopic mass current density of component 1, $\langle \mathbf{J}_Q \rangle$ is the macroscopic heat flux vector,

$\mathbf{X}_1$ is the thermodynamic force conjugate to $\langle \mathbf{J}_1 \rangle$, and $\mathbf{X}_Q$ is the force corresponding to the heat flow. The different $L_{\alpha\beta}$ are transport coefficients. The mass current can be expressed as

$$\langle \mathbf{J}_1 \rangle = \rho_1 (\langle \mathbf{v}_1 \rangle - \langle \mathbf{v} \rangle) , \tag{2.2}$$

where ρ_1 is the density of species 1, $\langle \mathbf{v}_1 \rangle$ is the center-of-mass velocity of species 1, and $\langle \mathbf{v} \rangle$ is the baryocentric velocity of the system. In a binary mixture the flux of component 2 $\langle \mathbf{J}_2 \rangle$ is simply equal to $-\langle \mathbf{J}_1 \rangle$. The other forces and fluxes can be defined in a few different ways. In this work we have used the following definitions:

$$\mathbf{X}_Q = -\frac{1}{T^2} \nabla T , \tag{2.3a}$$

$$\mathbf{X}_1 = -\nabla [(\mu_1 - \mu_2)/T] , \tag{2.3b}$$

where T is the absolute temperature and μ_α is the chemical potential of species α. The force conjugate to $\langle \mathbf{J}_2 \rangle, \mathbf{X}_2$ is equal to $-\mathbf{X}_1$. The Irving and Kirkwood [11] definition of the macroscopic heat current is

$$\langle \mathbf{J}_Q \rangle = \langle \mathbf{J}_e \rangle - (\rho \langle e \rangle \langle \mathbf{v} \rangle - \langle \mathsf{P} \rangle \cdot \langle \mathbf{v} \rangle) , \tag{2.4}$$

where ρ is the density of the fluid, $\langle e \rangle$ is the internal energy per particle, and $\langle \mathsf{P} \rangle$ is the pressure tensor. The current $\langle \mathbf{J}_e \rangle$ satisfies the energy continuity equation

$$\frac{\partial \rho \langle e \rangle}{\partial t} = -\nabla \cdot \langle \mathbf{J}_e \rangle . \tag{2.5}$$

The entropy production δ takes the form

$$\delta = \langle \mathbf{J}_Q \rangle \cdot \mathbf{X}_Q + \langle \mathbf{J}_1 \rangle \cdot \mathbf{X}_1 + \langle \mathbf{J}_2 \rangle \cdot \mathbf{X}_2 . \tag{2.6}$$

Given these definitions, the Onsager reciprocity relations state that $L_{Q1} = L_{1Q}$.

We will refer to L_{11} as the diffusion coefficient even though the mutual diffusion coefficient is defined as L_{11} multipled by a thermodynamic factor. The cross-coupling coefficients L_{1Q} and L_{Q1} will be referred to as the Soret and the Dufour coefficients, respectively. The relationship between the thermal conductivity λ and L_{QQ} is simply $\lambda = L_{QQ}/T^2$.

B. Microscopic theory

The system we simulate consists of N_1 particles of component 1 and mass m_1 and N_2 particles of component 2 and mass m_2. The total number of particles is $N = N_1 + N_2$. The volume of the system is V. The position coordinates and the momenta of particle i of species ν are denoted by $\mathbf{q}_i^\nu$ and $\mathbf{p}_i^\nu$, respectively, and $\mathbf{q}_{ij}^{\mu\nu} = \mathbf{q}_j^\nu - \mathbf{q}_i^\mu$ is the distance vector between particle i of species ν and particle j of species μ. The pair-interaction energy between these particles is denoted $\Phi_{ij}^{\mu\nu}$ and the force exerted on particle i by particle j is $F_{ij}^{\mu\nu}$. With these definitions we can write down the Irving and Kirkwood [11] expression for the microscopic heat current corresponding to the macroscopic expression in Eq. (2.4):

$$V\mathbf{J}_Q = \tfrac{1}{2} \sum_{\nu=1}^{2} \sum_{i=1}^{N_\nu} \left[\frac{\mathbf{p}_i^\nu}{m_\nu} - \mathbf{v} \right] \cdot \left\{ \left[m_\nu \left[\frac{\mathbf{p}_i^\nu}{m_\nu} - \mathbf{v} \right]^2 + \sum_{\mu=1}^{2} \sum_{j=1}^{N_\mu} \Phi_{ij}^{\mu\nu} \right] \mathsf{I} - \sum_{\mu=1}^{2} \sum_{j=1}^{N_\mu} \mathbf{q}_{ij}^{\mu\nu} \mathbf{F}_{ij}^{\mu\nu} \right\} , \tag{2.7}$$

where I is the unit tensor. The molecular form of the mass current Eq. (2.2) is simply

$$V\mathbf{J}_\nu = N_\nu m_\nu (\mathbf{v}_\nu - \mathbf{v}) , \tag{2.8}$$

where

$$N_\nu m_\nu \mathbf{v}_\nu = \sum_{i=1}^{N_\nu} \mathbf{p}_i^\nu .$$

With these definitions of the microscopic currents the Green-Kubo relations for the various transport coefficients in Eq. (2.1) can be expressed as

$$L_{11}\mathsf{I} = \frac{V}{k_B} \int_0^\infty dt \langle \mathbf{J}_1(t) \mathbf{J}_1(0) \rangle , \tag{2.9a}$$

$$L_{1Q}\mathsf{I} = \frac{V}{k_B} \int_0^\infty dt \langle \mathbf{J}_1(t) \mathbf{J}_Q(0) \rangle , \tag{2.9b}$$

$$L_{QQ}\mathsf{I} = \frac{V}{k_B} \int_0^\infty dt \langle \mathbf{J}_Q(t) \mathbf{J}_Q(0) \rangle , \tag{2.9c}$$

where k_B is Boltzmann's constant. These expressions are used when the transport coefficients are evaluated using EMD simulations. In this work, however, we are going to apply the EC NEMD algorithm for the heat flow and the color conductivity algorithm for the mutual diffusion coefficient. A brief discussion of Green-Kubo relations for mixtures is given in the Appendix.

The equations of motion for the EC heat-flow algorithm are

$$\dot{\mathbf{q}}_i^\nu = \frac{\mathbf{p}_i^\nu}{m_\nu} , \tag{2.10a}$$

$$\dot{\mathbf{p}}_i^\nu = \mathbf{F}_i + \left[\mathsf{S}_i^\nu - \frac{1}{N} \mathsf{S} + \frac{c_{h\nu}}{N} \mathsf{S} - k_B T c_{h\nu} \mathsf{I} \right] \cdot \mathcal{F}_Q - \alpha (\mathbf{p}_i^\nu - \bar{\mathbf{p}}_\nu) , \tag{2.10b}$$

where

$$\mathsf{S}_i^n = \frac{1}{2} \left[m_\nu \left[\frac{\mathbf{p}_i^\nu}{m_\nu} - \mathbf{v} \right]^2 + \sum_{\mu=1}^{2} \sum_{j=1}^{N_\mu} \Phi_{ij}^{\mu\nu} \right] \mathsf{I} - \frac{1}{2} \sum_{\mu=1}^{2} \sum_{j=1}^{N_\mu} \mathbf{q}_{ij}^{\mu\nu} \mathbf{F}_{ij}^{\mu\nu} ,$$

$$\bar{\mathbf{p}}_\nu = \frac{1}{N_\nu} \sum_{i=1}^{N_\nu} \mathbf{p}_i^\nu$$

and

$$\mathbf{S}=\sum_{\nu=1}^{2}\sum_{i=1}^{N_\nu}\mathbf{S}_i^\nu .$$

The values of the color charges $c_{h\nu}$ are obtained by requiring color neutrality of the system, i.e., $N_1c_{h1}+N_2c_{h2}=0$, and momentum conservation. This gives

$$c_{h1}=N_2(m_2-m_1)/(N_1m_1+N_2m_2)$$

and

$$c_{h2}=-N_1(m_2-m_1)/(N_1m_1+N_2m_2) .$$

Note that the color charges become zero if the masses of the two species are equal. The multiplier α is determined by applying Gauss's principle [12] together with the kinetic-energy $E_{\rm kin}$ constraint,

$$\dot{E}_{\rm kin}=\frac{d}{dt}\sum_{\nu=1}^{2}\frac{1}{2m_\nu}\sum_{i=1}^{N_\nu}(\mathbf{p}_i^\nu-\bar{\mathbf{p}}_\nu)^2=0 . \tag{2.11}$$

The mean mass current per particle of the component in question $\bar{\mathbf{p}}_\nu$ is deducted from the momenta in the expression for $E_{\rm kin}$ in order to prevent the thermostat from interfering with the mass currents. One obtains the following expression for α:

$$\alpha=\frac{\sum_{\nu=1}^{2}\frac{1}{m_\nu}\sum_{i=1}^{N_\nu}(\mathbf{p}_i^\nu-\bar{\mathbf{p}}_\nu)\cdot\left[\mathbf{F}_i+\left[\mathbf{S}_i^\nu-\frac{1}{N}\mathbf{S}+\frac{c_{h\nu}}{N}\mathbf{S}-k_BTc_{h\nu}\mathbf{l}\right]\cdot\mathcal{F}_Q\right]}{\sum_{\nu=1}^{2}\frac{1}{m_\nu}\sum_{i=1}^{N_\nu}(\mathbf{p}_i^\nu-\bar{\mathbf{p}}_\nu)^2} . \tag{2.12}$$

By setting $\alpha=0$ one recovers the adiabatic equations of motion.

The general idea when one constructs NEMD algorithms is to devise equations of motion in such a way that the time derivative of the adiabatic field-free Hamiltonian $H_0^{\rm ad}$ is equal to the scalar product of the flux $\mathbf{J}$ and some force $\mathcal{F}$:

$$\dot{H}_0^{\rm ad}=\sum_{k=1}^{N}\dot{\mathbf{p}}_i\cdot\frac{\mathbf{p}_i}{m_i}-\mathbf{F}_i\cdot\dot{\mathbf{q}}_i=-V\mathbf{J}\cdot\mathcal{F} . \tag{2.13}$$

If the algorithm satisfies adiabatic incompressibility of phase space (AIΓ), i.e.,

$$\Lambda^{\rm ad}=\sum_{i=1}^{N}\frac{\partial\dot{\mathbf{q}}_i^{\rm ad}}{\partial\mathbf{q}_i}+\frac{\partial\dot{\mathbf{p}}_i^{\rm ad}}{\partial\mathbf{p}_i}=0 , \tag{2.14}$$

where $\Lambda^{\rm ad}$ is the phase-space compression factor and $\dot{\mathbf{p}}$ and $\dot{\mathbf{q}}$ should be taken from the adiabatic equations of motion, one can show that [12] the linear response of a phase variable B is given by

$$\langle B(t)\rangle=\langle B(0)\rangle-\beta V\int_0^t dt'\langle B(t')\mathbf{J}(0)\rangle\cdot\mathcal{F} , \tag{2.15}$$

where $\beta=1/k_BT$ and t is the time that has elapsed after the force $\mathcal{F}$ was turned on. The best way of utilizing this relation is to find some equations of motion such that $\mathbf{J}$ becomes one of the currents appearing in the GK relation for the transport coefficient in question. Then, by letting B be the other current in the GK relation one can evaluate the nonequilibrium steady-state GK relation by monitoring B. The equilibrium GK integral and the transport coefficients are obtained in the limit of zero $\mathcal{F}$. When one has a heat-flow algorithm $\mathbf{J}$ should become $\mathbf{J}_Q$. This gives the following expressions for L_{QQ} and L_{1Q}:

$$L_{QQ}=\lim_{\mathcal{F}_Q\to0}M_{QQ}=\lim_{\mathcal{F}_Q\to0}\lim_{t\to\infty}\frac{T\langle J_Q(t)\rangle}{\mathcal{F}_Q} \tag{2.16a}$$

and

$$L_{1Q}=\lim_{\mathcal{F}_Q\to0}M_{1Q}=\lim_{\mathcal{F}_Q\to0}\lim_{t\to\infty}\frac{T\langle J_1(t)\rangle}{\mathcal{F}_Q} , \tag{2.16b}$$

where $\mathcal{F}_\alpha=|\mathcal{F}_\alpha|$ and $J_\alpha=|\mathbf{J}_\alpha|$.

The EC algorithm conserves momentum but AIΓ is not satisfied:

$$\Lambda^{\rm ad}=(1/m_1-1/m_2)\mathbf{J}_1\cdot\mathcal{F}_Q .$$

It is only zero if the masses of the two species are the same. The time derivative of the adiabatic Hamiltonian $dH_0^{\rm ad}/dt=(1/m_1-1/m_2)\mathbf{J}_1\cdot\mathcal{F}_Q+\mathbf{J}_Q\cdot\mathcal{F}_Q$, whereas one would like it to be equal to $\mathbf{J}_Q\cdot\mathcal{F}_Q$. For these two reasons one might think that it would be impossible to find a linear-response relation like Eq. (2.15). However, Evans and Cummings showed that for the linear response the $\Lambda^{\rm ad}$ term exactly cancels the additional unwanted term involving $\mathbf{J}_1\cdot\mathcal{F}_Q$ in the dissipation. Thus the Evans-Cummings equations yield the correct GK relation.

The color conductivity algorithm that we use employs the following equations of motion:

$$\dot{\mathbf{q}}_i^\nu=\frac{\mathbf{p}_i^\nu}{m_\nu} , \tag{2.17a}$$

$$\dot{\mathbf{p}}_i^\nu=\mathbf{F}_i+c_\nu\mathcal{F}_D-\alpha(\mathbf{p}_i^\nu-\bar{\mathbf{p}}_\nu) , \tag{2.17b}$$

where c_ν is the color charge of component ν, $\mathcal{F}_D$ is the color force, and

$$\alpha=\frac{\sum_{\nu=1}^{2}\frac{1}{m_\nu}\sum_{i=1}^{N_\nu}(\mathbf{p}_i^\nu-\bar{\mathbf{p}}_\nu)\cdot\mathbf{F}_i}{\sum_{\nu=1}^{2}\frac{1}{m_\nu}\sum_{i=1}^{N_\nu}(\mathbf{p}_i^\nu-\bar{\mathbf{p}}_\nu)^2} , \tag{2.18}$$

the Gaussian multiplier that maintains $E_{\rm kin}$ constant.

Equations (2.17b) and (2.18) are derived from Gauss's principle and the kinetic-energy constraint (2.12). The color charges c_ν must satisfy the color-charge-neutrality condition $N_1c_1+N_2c_2=0$ in order to conserve the linear momentum. In this work this has been done by setting $c_1=N/N_2$ and $c_2=-N/N_1$. From linear-response theory and the GK relations one can obtain the following transport coefficients:

$$L_{11}=\lim_{\mathcal{F}_D\to 0} M_{11}=\lim_{\mathcal{F}_D\to 0}\lim_{t\to\infty}\frac{T\langle J_1(t)\rangle}{\left[\frac{N}{N_1m_1}+\frac{N}{N_2m_2}\right]\mathcal{F}_D} \tag{2.19a}$$

and

$$L_{Q1}=\lim_{\mathcal{F}_D\to 0} M_{Q1}=\lim_{\mathcal{F}_D\to 0}\lim_{t\to\infty}\frac{T\langle J_Q(t)\rangle}{\left[\frac{N}{N_1m_1}+\frac{N}{N_2m_2}\right]\mathcal{F}_D}\,. \tag{2.19b}$$

C. Technical details

In this work we consider a binary equimolar LJ mixture. In such a system a particle of species μ interacts with another particle of species ν via the following pair potential:

$$u_{\mathrm{LJ}}=4\varepsilon_{\mu\nu}\left[\frac{\sigma_{\mu\nu}^{12}}{r^{12}}-\frac{\sigma_{\mu\nu}^{6}}{r^{6}}\right], \tag{2.20}$$

where $\sigma_{\mu\nu}$ is the zero of the potential, $\varepsilon_{\mu\nu}$ is the depth of the attractive minimum, and $r=|\mathbf{q}^\mu-\mathbf{q}^\nu|$, the scalar distance between the particles. In order to decrease the computational effort, the potential has been truncated:

$$u(r)=\begin{cases} u_{\mathrm{LJ}}(r)-u_{\mathrm{LJ}}(r_c)\,, & r<r_c \\ 0\,, & r\geq r_c \end{cases} \tag{2.21}$$

the parameter r_c being the cutoff radius beyond which the interaction potential is set equal to zero. The different parameters in the potential have been chosen to model an argon-krypton (denoted 1-2) mixture with $\sigma_{11}=3.405$ Å, $\sigma_{22}=3.633$ Å, $\varepsilon_{11}/k_B=119.6$ K, $\varepsilon_{22}/k_B=167.0$ K, $\sigma_{12}=(\sigma_{11}+\sigma_{22})/2$, and $\varepsilon_{12}=(\varepsilon_{11}\varepsilon_{22})^{1/2}$. The potential was truncated at $r_c=2.5\sigma_{\mu\nu}$, i.e., the cutoff radii are slightly different for the different kinds of interactions. The masses of the two different species are $m_1=39.95$ u, $m_2=83.80$ u. The LJ diameter and the mass of the argon atom σ_{11} and m_1 have been used as length units and mass units, respectively. The time unit τ has been taken to be $\sigma_{11}(m_1/\varepsilon_{11})^{1/2}$ which is equal to about 2 ps. In order to simplify the following discussion we will refer to a LJ fluid where the potential parameters have been chosen to model argon, krypton, or argon-krypton mixtures as closely as possible, even though this is a rather crude approximation. A LJ fluid where the potential parameters have been chosen more or less at random will be referred to as a "hypothetical fluid."

The state point has been chosen to be close to the argon-krypton triple point. All the transport coefficients of this system have been studied comprehensively by a number of workers [2,3,8,9] and in addition the mutual diffusion coefficient has also been calculated several times [13,14]. The reduced temperature k_BT/ε_{11} is equal to 0.9650 and the reduced density $N\sigma_{11}^3/V$ is equal to 0.7137.

The equations of motion were integrated using a fourth-order gear predictor corrector method. For low heat fields $\mathcal{F}_Q<0.5$ and all the color fields we have used a time step of 0.004τ, but for the larger heat fields we decreased the time step to 0.002τ. The correctness of the program has been tested in various ways. First, M_{11} from the color current algorithm should agree with the value of this quantity in Ref. [2]. This has been found to be the case. Second, we have also performed EMD simulations to evaluate the GK expressions for the various transport coefficients in Eq. (2.9). The GK relations give fairly accurate estimates of M_{QQ} and M_{11}. These coefficients agree within the statistical uncertainty with the NEMD results. Third, we have also performed some calculations at constant internal energy rather than constant kinetic energy. The isokinetic heat-flow algorithm Eqs. (2.10) can be converted to an isoenergetic algorithm by using a slightly different expression for the multiplier α:

$$\alpha=\frac{\sum_{\nu=1}^{2}\left[\frac{1}{m_\nu}\sum_{i=1}^{N_\nu}[\mathbf{p}_i^\nu-\bar{\mathbf{p}}_\nu]\cdot\left[\mathbf{S}_i^\nu-\frac{1}{N}\mathbf{S}+\frac{c_{h\nu}}{N}\mathbf{S}-k_BTc_{h\nu}\mathbf{I}\right]\cdot\mathcal{F}_Q+\bar{\mathbf{p}}_\nu\cdot\mathbf{F}_i\right]}{\sum_{\nu=1}^{2}\frac{1}{m_\nu}\sum_{i=1}^{N_\nu}(\mathbf{p}_i^\nu-\bar{\mathbf{p}}_\nu)^2}\,. \tag{2.22}$$

The internal energy was simply set equal to its average value from an isokinetic simulation. The fact that when α is set to this value energy is conserved constitutes a significant internal consistency check. The constant energy simulation results for the temperature and the different currents coincided very well with the isokinetic values.

III. RESULTS AND DISCUSSION

We have calculated transport coefficients for a Lennard-Jones mixture by NEMD molecular dynamics for two systems, one with 108 particles and another one with 1024 particles. We have also performed EMD simulations for the smaller system to evaluate the GK integrals

TABLE I. Thermal conductivity simulations.

	Length (in units of τ)	
$\lvert\mathcal{F}_Q\rvert$	$N=108$	$N=1024$
0.075		4400
0.100	20000	3600
0.150	4000	2400
0.200	4000	2600
0.300	4000	800
0.400	4000	800
0.500	4000	
0.600	2000	
0.800	2000	
1.000	600	
1.200	1120	
1.500	560	
2.000	400	
2.500	500	
3.000	500	
3.500	1000	
4.000	280	

in order to provide a consistency check. In Tables I and II we list the run lengths in units of τ for the different heat fields and color fields. When the external field is small, fairly long runs are required to achieve a reasonable statistical accuracy for the various transport coefficients. When the external field increases the fluctuations are relatively small so the run times can be shortened. The error bars in the figures in this section were obtained by dividing the simulation run into four equal parts and calculating the standard deviation of the subaverages. The proper way of applying NEMD methods for the evaluation of different transport coefficients is to compute them at a few different external fields and extrapolate to zero field. Unfortunately, this is very hard to do because the signal-to-noise ratio decreases with the field. Therefore we have performed moderately long simulation runs for the larger fields and one very long run for the lowest field where it is at all possible to obtain reasonable results, we quote this value as the value for the transport coefficient in question.

In Fig. 1 we have plotted M_{QQ} as a function of the heat field $\mathcal{F}_Q$ for the two different systems. In the linear regime the difference is rather small but M_{QQ} is a little larger in the larger system. When the field increases M_{QQ} starts to rise earlier and more steeply in the larger system. This system-size dependence has also been found to be the case in two-dimensional one-component soft-disk systems [15]. In the limit of an infinite system it has been proved that the conductivity is infinite for any finite heat field [16]. (We note in passing that similar effects occur for every other transport process, except that the system-size dependence is more easily seen for thermal conductivity.) The behavior of M_{QQ} in the smaller system can be divided into three regimes. When $0 \le |\mathcal{F}_Q| < 0.5$ one has a relatively weakly nonlinear regime where M_{QQ} is approximately equal to 4.2. Then in the interval $0.5 \le \mathcal{F}_Q < 1.5$ M_{QQ} rapidly increases to a maximum of about 7.8 after which it levels off and starts diminishing again. The value of M_{QQ} at small fields is about 4.10 ± 0.03 for $|\mathcal{F}_Q| = 0.100$ and 4.24 ± 0.01 for $|\mathcal{F}_Q| = 0.075$ for the small and large systems, respectively.

In Fig. 2 the simulation results for M_{11} as a function of the color field $\mathcal{F}_D$ are shown. M_{11} increases monotonously with the color field until a phase transition takes place. The system then separates into two different phases consisting of either species and it becomes unstable [17]. The

TABLE II. Mutual diffusion simulations.

	Length (in units of τ)	
$\lvert\mathcal{F}_D\rvert$	$N=108$	$N=1024$
0.35		5200
0.50	20000	3200
0.75	4000	1600
1.00	4000	
1.25	2900	
1.50	2400	
2.00	3100	

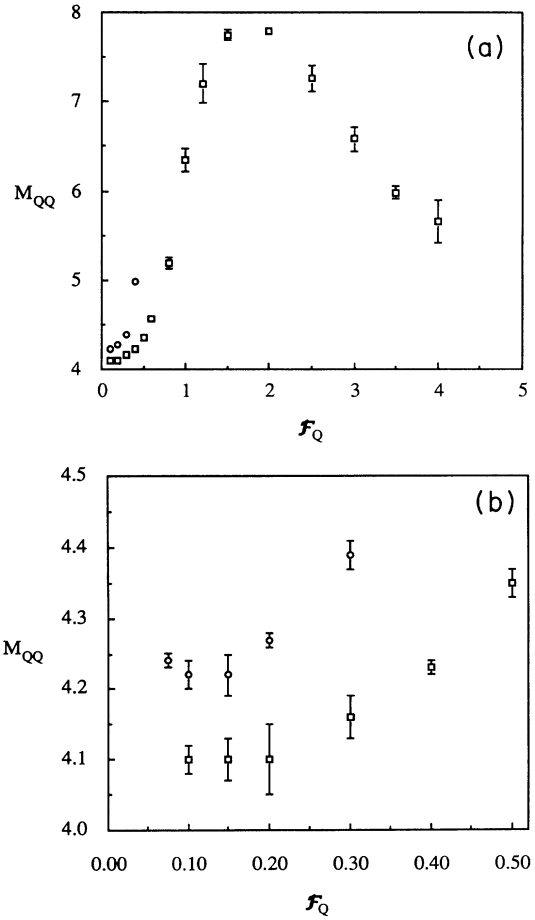

FIG. 1. The thermal conductivity M_{QQ} as a function of the heat field $\mathcal{F}_Q$. Squares and circles represent the 108- and 1024-particle systems, respectively. If there are no error bars this means that they are not visible on the scale of the figure. (a) The whole range of $\mathcal{F}_Q$. (b) Detail for small values of the heat field.

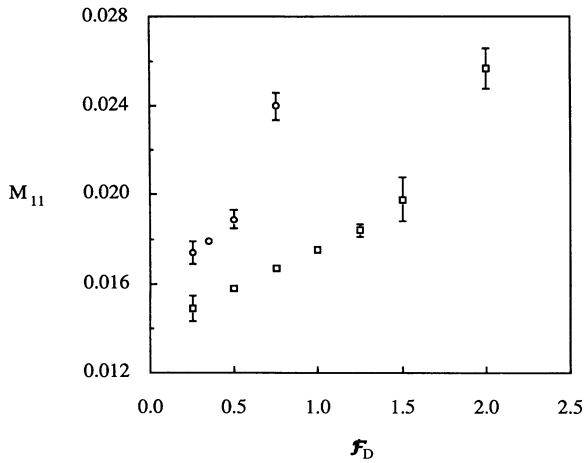

FIG. 2. The mutual diffusion coefficient M_{11} as a function of the color field $\mathcal{F}_D$. Same symbols as in Fig. 1.

transition point is $|\mathcal{F}_D| \approx 2.5$ in the small system and $|\mathcal{F}_D| \approx 1.0$ in the large system. In the small system it is very tempting to draw a straight line through data points to obtain the extrapolated value of M_{11}. Unfortunately, the error bar of the data point for the smallest color field is fairly large, which makes it impossible to rule out a turning point. In addition one would obtain a very low value of the diffusion coefficient and there is no theoretical justification for a linear behavior either, so we refrain from this kind of extrapolation. Over the whole range of the color field M_{11} is greater in the larger system. This observation can resolve the difference in M_{11} between Ref. [2], which agrees with our results, and Ref. [14]. The value of M_{11} is about 15% lower in the former work where 108 particles were used than in the latter work utilizing 864 particles, so the apparent difference is probably a system-size effect. Our values of M_{11} at small color fields are 0.0149 ± 0.0006 for $|\mathcal{F}_D| = 0.500$ in the 108-particle system and 0.0174 ± 0.0005 for $|\mathcal{F}_D| = 0.350$ in the 1024-particle system.

In Fig. 3 the dependence of the cross-coupling coefficient M_{1Q} upon $\mathcal{F}_Q$ is displayed. This coefficient is negative, which means that if there is a temperature gradient in an argon-krypton mixture then argon will slowly move toward the warmer regions and krypton toward the cooler areas. In the small system the absolute value of M_{1Q} decreases as the field increases. When the heat field is small, i.e., $|\mathcal{F}_D| < 1.5$, the field increases faster than M_{1Q} falls off, so the mass current $\mathbf{J}_1 = M_{1Q}\mathcal{F}_Q$ induced by the heat flow increases to a maximum. After that the field cannot compensate for the decreasing magnitude of the cross-coupling coefficient so the mass current becomes smaller for larger fields. As one can see from Fig. 3(b) the error bars make it impossible to discern any system-size dependence. The small-field result for the cross-coupling coefficient is 0.0155 ± 0.002 for $|\mathcal{F}_Q| = 0.100$ in the smaller system and 0.0182 ± 0.001 for $|\mathcal{F}_Q| = 0.075$ in the large system.

Finally in Fig. 4 we have plotted the other cross-coupling coefficient M_{Q1} as a function of the color field. It is negative for small fields but (in the 108-particle system) it increases and changes sign and becomes positive as $\mathcal{F}_D$ increases. This is probably due to the onset of the phase separation that occurs at higher fields. Also in this case the error bars make it impossible to find any system-size dependence. The low-field value of this cross-coupling coefficient is 0.0156 ± 0.002 for $|\mathcal{F}_D| = 0.50$ in the small system and 0.0167 ± 0.002 for $|\mathcal{F}_D| = 0.35$ in the larger system. Note that in the linear region $M_{Q1} = M_{1Q}$ within the statistical uncertainty both for the large system and the small system. Thus the Onsager reciprocity relations are satisfied. All the results for the different transport coefficients in this section for the 108-particle system agree very well with the NEMD simulation values given in Ref. [2]. For the color conductivity algorithm this is just a check of the computer program. It is not surprising that the EC algorithm gives the same result as the ME algorithm for an argon-krypton mixture because this system is almost ideal.

We have also used the EC heat flow algorithm to calculate the cross-coupling coefficient M_{1Q} for three hypothetical LJ mixtures. We performed simulations of the 108-particle system where the heat field is set equal to 0.100 and the run length was $10\,000\tau$. This is the small-

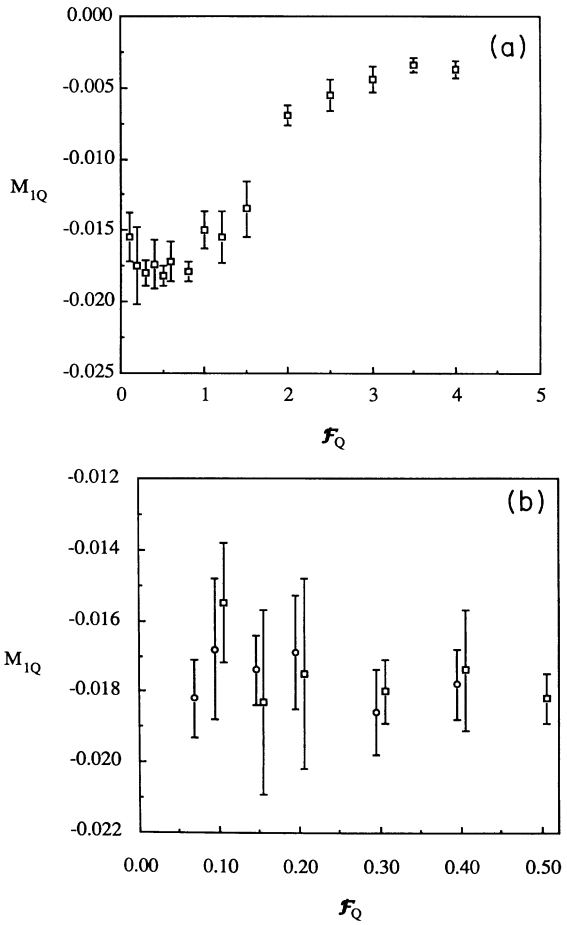

FIG. 3. The cross-coupling coefficient M_{1Q} as a function of the heat field $\mathcal{F}_Q$. Same symbols as in Fig. 1. (a) The whole range of $\mathcal{F}_Q$. (b) Detail for small values of the heat field.

est field that we used for the argon-krypton system and half the run time for that system at that field. The first hypothetical system we tried was the same system as above but we set the mass of krypton equal to the mass of argon; the other potential parameters were unchanged and the state point was still close to the triple point. This is of particular interest for two reasons. First, when the masses of either species is equal the EC heat-flow algorithm satisfies AIΓ. The second reason is that in a binary mixture the component with the lowest molecular weight usually diffuses towards the warmer regions [18], but now when the masses are equal it will be very hard to determine where the two components will diffuse. The value of the cross-coupling coefficient was found to be 0.022 ± 0.002. It is interesting to note that the cross-coupling coefficient has changed sign. Thus if the mass of krypton is decreased the induced mass currents will decrease and eventually they will change directions. The second system was the same as the argon-krypton mixture, except for that the diameters of krypton σ_{22} and σ_{12} were equal to the diameter of argon σ_{11}. In this case M_{1Q} was equal to -0.032 ± 0.006. This means that the sign is retained but the magnitude is greater. Finally we tried a mixture where the potential minima of the krypton-krypton and the krypton-argon interactions ε_{22} and ε_{12} in the LJ potential were equal to that of the argon-argon interaction ε_{11}, but all the other parameters were left unchanged. This gave the value -0.034 ± 0.002 for M_{1Q}. The conclusion that can be drawn from these three calculations is that the triple-point argon-krypton mixture has a very small cross-coupling coefficient, and if one is interested in studying the details of thermal diffusion it is worthwhile to look at more nonideal systems.

In order to provide an independent consistency check for our program we also performed an EMD simulation to calculate the different current correlation functions, which we have used to evaluate the GK integrals for the various transport coefficients. We simulated the 108-particle system for 40 000 units of τ with a time step of 0.004τ. The heat flow and the mass current autocorrelation functions, i.e., $C_{QQ}(t)=\langle \mathbf{J}_Q(t)\mathbf{J}_Q(0)\rangle$ and $C_{11}(t)=\langle \mathbf{J}_1(t)\mathbf{J}_1(0)\rangle$, which can be seen in Fig. 5, are fairly easy to calculate. They decay to zero and remain zero for more than six units of τ. This is roughly the time during which the numerically obtained solution to the equations of motion are reversible. Thus if a GK relation should be useful, the integrals of the tails of the correlation functions must have converged in a time less than $\sim 6\tau$. The values of the time integrals of $C_{11}(t)$ and $C_{QQ}(t)$,

$$I_{11}(t)=\frac{V}{k_B}\int_0^t dt' C_{11}(t') \tag{3.1a}$$

and

$$I_{QQ}(t)=\frac{V}{k_B}\int_0^t dt' C_{QQ}(t') , \tag{3.1b}$$

which are equal to L_{11} and L_{QQ} in the limit of infinite time, have converged after $t=1.0\tau$ and they remain virtually constant, at least until $t=6\tau$. The value of I_{11} is 0.0160 ± 0.0001 for $t=5\tau$ and 0.0159 ± 0.0001 for $t=6\tau$. The corresponding values for I_{QQ} are 4.11 ± 0.02 and 4.12 ± 0.02. The error bars have been calculated by dividing the simulation into four equal parts and then comput-

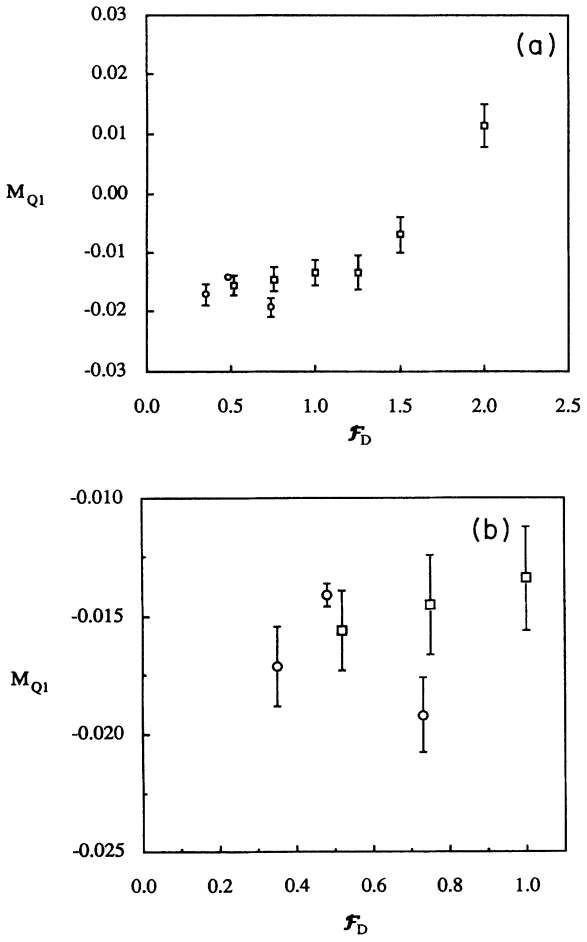

FIG. 4. The mutual diffusion coefficient M_{Q1} as a function of the color field $\mathcal{F}_D$. Same symbols as in Fig. 1. (a) The whole range of $\mathcal{F}_D$. (b) Detail for small values of the color field.

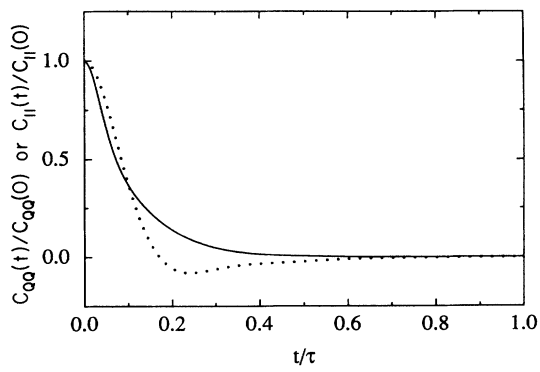

FIG. 5. The normalized heat current autocorrelation function $C_{QQ}(t)/C_{QQ}(0)$ (solid curve) and the normalized mass current autocorrelation function $C_{11}(t)/C_{11}(0)$ (dashed curve) as functions of time.

ing the standard deviations of the subaverages. These values agree very well with the NEMD results.

The situation is considerably worse for the cross-correlation functions $C_{Q1}(t)=\langle \mathbf{J}_Q(t)\mathbf{J}_1(0)\rangle$ and $C_{1Q}(t)=\langle \mathbf{J}_1(t)\mathbf{J}_Q(0)\rangle$. These quantities are displayed in Fig. 6(a). They should be the same at all times, but they already start deviating from each other at 0.25τ and the tails are completely lost in the noise. It is obvious that simulation runs orders of magnitude longer than this one are required to obtain the same accuracy as for the autocorrelation functions. The time integrals of these cross-correlation functions

$$I_{1Q}(t)=\frac{V}{k_B}\int_0^t dt' C_{1Q}(t') \tag{3.2a}$$

and

$$I_{Q1}(t)=\frac{V}{k_B}\int_0^t dt' C_{Q1}(t') \tag{3.2b}$$

can be seen in Fig. 6(b). In the long-time limit these integrals are equal to L_{1Q} and L_{Q1}. There are considerable statistical deviations between $I_{1Q}(t)$ and $I_{Q1}(t)$ for times larger than 1.0τ. In Table III we display values of $I_{1Q}(t)$ and $I_{Q1}(t)$ for t between 1.0τ and 3.0τ. The error bars have been obtained in the same way as those of the integrals of the autocorrelation functions. It is obvious that one can obtain values of the cross-coupling coefficients between -0.015 and -0.020 by choosing t differently in Eq. (3.2). This interval is largely the same as that obtained from the NEMD simulations. If we take half of this interval to be the error and if we take the average of the values in Table III as the value of I_{1Q} and I_{Q1} we obtain -0.0173 ± 0.0025.

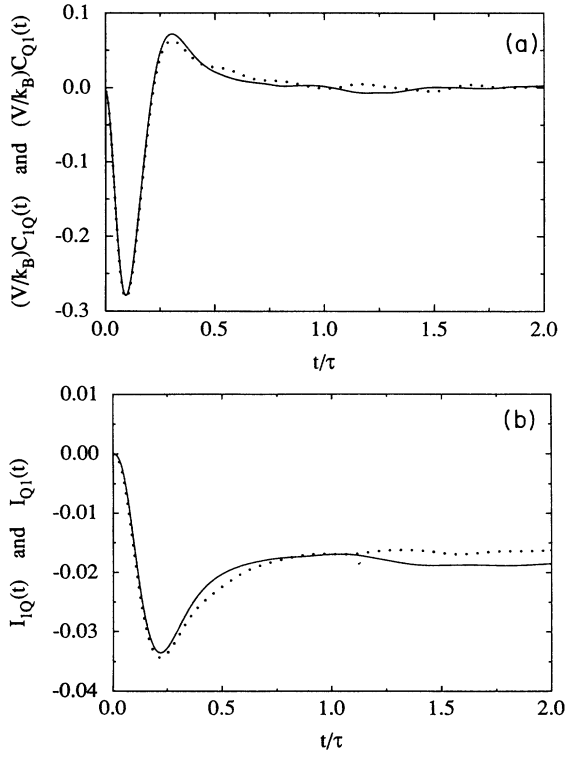

FIG. 6. (a) The cross correlation functions $(V/k_B)C_{1Q}(t)$ (solid curve) and $(V/k_B)C_{Q1}(t)$ (dotted curve) as functions of time. (b) The time integrals from zero to time t of $(V/k_B)C_{1Q}(t), I_{1Q}(t)$ (solid curve) and of $(V/k_B)C_{Q1}(t), I_{Q1}(t)$ (dotted curve).

TABLE III. $I_{1Q}(t)$ and $I_{Q1}(t)$.

t/τ	$I_{1Q}(t)$	$I_{Q1}(t)$
1.0	-0.017 ± 0.005	-0.017 ± 0.0005
1.5	-0.019 ± 0.001	-0.017 ± 0.001
2.0	-0.019 ± 0.001	-0.016 ± 0.001
2.5	-0.019 ± 0.001	-0.016 ± 0.001
3.0	-0.017 ± 0.001	-0.016 ± 0.001

IV. CONCLUSION

In this work we have used the Evans-Cummings NEMD heat-flow algorithm to calculate the thermal conductivity and the Soret coefficient in a binary Lennard-Jones mixture. We have chosen the different potential parameters in such a way that the system should resemble an argon-krypton mixture. We chose the state point to be the triple point of an equimolar mixture, mainly because this system has been studied by a number of other workers and thus comparisons will be facilitated. In order to provide consistency checks we used the color conductivity algorithm to calculate the Dufour coefficient and the mutual diffusion coefficient. According to the Onsager reciprocity relations, the Dufour and the Soret coefficients should be equal. We also calculated the cross-coupling coefficients for three hypothetical types of Lennard-Jones mixtures. Finally we performed an EMD simulation to compute the Green-Kubo expressions for the various transport coefficients.

Formerly, the only *general* way of obtaining the thermal conductivity and the cross-coupling coefficients of simple fluid mixtures was through evaluation of the appropriate GK relations. There was one NEMD algorithm available devised by McGowan and Evans, but it was only strictly valid for ideal mixtures.

We have studied one small system and one large system consisting of 108 and 1024 particles, respectively. Our NEMD results for the small system for the four different transport coefficients mentioned above all agree with the ME values. This is not unexpected because an argon-krypton mixture is almost ideal. The Soret and the Dufour coefficients also coincide within the statistical uncertainties, so the Onsager reciprocity relations are satisfied. The cross-coupling coefficients were negative, which means that argon moves toward warmer regions and krypton toward cooler regions. When the system size increases the thermal conductivity and the diffusion coefficient increase slightly but the statistical noise makes it very hard to determine whether there are any system-size effects of the cross-coupling coefficients.

We also studied three hypothetical equimolar LJ mixtures. They were all derived from the triple-point argon-krypton mixture by either changing the mass of krypton

or one of the LJ potential parameters, but the number density and the temperature were left unchanged. In the first case we set the mass of krypton equal to the argon mass, in the second case the diameter of krypton was set equal to that of argon, and in the third case the depths of the potential minimum of the krypton-krypton interaction was set equal to that of argon. In the equal-mass case the Soret coefficient changed sign and became positive, but in the two other types of mixtures the cross-coupling coefficient retained its sign and its magnitude increased slightly. The EMD Green-Kubo results for the thermal conductivity and the diffusion coefficient agree very well with the NEMD values. However, the GK results for the cross-coupling coefficient were very inaccurate. In order to evaluate the GK integrals accurately the tails of the correlation functions must be known accurately, but we did not manage to obtain reasonable statistics for these tails even though we performed a very long simulation. We estimate that the error of the GK cross coefficient values are as high as 15%.

The EC heat-flow method is the first NEMD algorithm that violates AIΓ. It has been argued that this will render the algorithm useless [19]. However, we did not encounter any problems that can be attributed to this violation. The adiabatic contribution is very small because it is proportional to the mass current induced by the heat flow, and as we have seen, the coupling between the heat flow and the mass current is rather weak.

ACKNOWLEDGMENT

One of us (D.J.E.) thanks Peter Cummings for a helpful discussion when the EC algorithm was developed.

APPENDIX

There are a number of alternative definitions of the heat-flux vector for mixtures. Depending on the particular problems being considered, one or another of these alternative definitions may turn out to be the most useful. Each of the different definitions of the heat flux vector carries with it a corresponding redefinition of the conjugate thermodynamic forces and the phenomenological transport coefficients. Different but equivalent Green-Kubo relations hold for each of these thermodynamic definitions.

The single-primed heat-flux vector used recently by Pomeau [20] is defined in terms of our unprimed Irving-Kirkwood heat-flux vector by the equation

$$\langle \mathbf{J}'_Q \rangle \equiv \langle \mathbf{J}_Q \rangle - \sum_\nu \mu_\nu \langle \mathbf{J}_\nu \rangle \ . \tag{A1}$$

More frequently we meet the Bearman-Kirkwood or the double-prime heat-flux vector [1],

$$\langle \mathbf{J}''_Q \rangle \equiv \langle \mathbf{J}_Q \rangle - \sum_\nu h_\nu \langle \mathbf{J}_\nu \rangle \ , \tag{A2}$$

where h_ν is the partial specific enthalpy of species ν.

The unprimed variables which we use in this work are instantaneous versions of the ensemble averaged expression for the heat-flux vector given by Irving and Kirkwood [11]. For a discussion of the relationship of the instantaneous and the ensemble-average Irving-Kirkwood forms for the Navier-Stokes fluxes, see Chapter 3 of Ref. [12].

The Irving-Kirkwood form for the heat-flux vector represents the nonconvective energy flux measured experimentally, and it is convenient in both experiment and computer simulation because it does not require a knowledge of difficult to measure quantities such as the partial enthalpies or the chemical potential.

Green [21] derived Green-Kubo relations for the transport coefficients in the single-primed description while Zubarev [22] and Wood [23] have given the corresponding relations for the unprimed description.

It is straightforward but tedious to show that Wood's unprimed heat-flux vector is the same as that given in our Eq. (2.7). Expansion of (2.7) gives

$$\mathbf{J}_Q V = \sum_i \mathbf{v}_i \hat{e}_i - \tfrac{1}{2} \sum_{\substack{i,j \\ i \neq j}} \mathbf{v}_i \cdot \mathbf{F}_{ij} \mathbf{r}_{ij} - \mathbf{v} \cdot \left[\sum_i \hat{e}_i \mathsf{I} + \sum_i m_i (\mathbf{v}_i - \mathbf{v})(\mathbf{v}_i - \mathbf{v}) - \tfrac{1}{2} \sum_{\substack{i,j \\ i \neq j}} \mathbf{F}_{ij} \mathbf{r}_{ij} \right] , \tag{A3}$$

where

$$\hat{e}_i \equiv \tfrac{1}{2} m v_i^2 + \tfrac{1}{2} \sum_j \phi_{ij} \tag{A4}$$

is the contribution of particle i to the *laboratory* energy of the system. For systems close to equilibrium, where local thermodynamic equilibrium holds, (A3) is the same as Eqs. (23) and (25) of Wood's paper [23]. (See also p. 305 of Ref. [24].)

Another equivalent form for the unprimed heat-flux vector is

$$\mathbf{J}_Q V = \sum_i \mathbf{v}_i e_i - \tfrac{1}{2} \sum_{\substack{i,j \\ i \neq j}} \mathbf{v}_i \cdot \mathbf{F}_{ij} \mathbf{r}_{ij} - \mathbf{v} \cdot \left[\sum_i e_i \mathsf{I} + \sum_i m_i (\mathbf{v}_i - \mathbf{v})(\mathbf{v}_i - \mathbf{v}) - \tfrac{1}{2} \sum_{\substack{i,j \\ i \neq j}} \mathbf{F}_{ij} \mathbf{r}_{ij} \right] - \mathbf{v} \tfrac{1}{2} \rho v^2 V \ , \tag{A5}$$

where e_i is the instantaneous contribution of particle i to the *internal* energy of the system:

$$e_i \equiv \tfrac{1}{2} m_i (\mathbf{v}_i - \mathbf{v})(\mathbf{v}_i - \mathbf{v}) + \tfrac{1}{2} \sum_j \phi_{ij} \ . \tag{A6}$$

Under local thermodynamic equilibrium (A5) reduces to

$$\mathbf{J}_Q V = \sum_i \mathbf{v}_i e_i - \tfrac{1}{2} \sum_{\substack{i,j \\ i \neq j}} \mathbf{v}_i \cdot \mathbf{F}_{ij} \mathbf{r}_{ij} - \mathbf{v} \cdot (h + \tfrac{1}{2} \rho v^2) V \ , \tag{A7}$$

where h is the instantaneous expression for the enthalpy per unit volume.

[1] S. R. de Groot and P. Mazur, *Nonequilibrium Thermodynamics* (Dover, New York, 1984).
[2] D. McGowan and D. J. Evans, Phys. Rev. A **34**, 2133 (1986); D. J. Evans and D. McGowan, *ibid.* **36**, 948 (1987).
[3] G. V. Paolini and G. Ciccotti, Phys. Rev. A **36**, 5156 (1987).
[4] G. Ciccotti, G. Jaccuci, and I. R. MacDonald, J. Stat. Phys. **21**, 1 (1979).
[5] D. McGowan, Phys. Rev. A **36**, 1367 (1987).
[6] J. J. Erpenbeck, Phys. Rev. A **39**, 4718 (1989).
[7] R. Vogelsang and C. Hoheisel, J. Chem. Phys. **89**, 1588 (1988).
[8] R. Vogelsang, C. Hoheisel, G. V. Paolini, and G. Ciccotti, Phys. Rev. A **36**, 3964 (1987).
[9] P. J. Gardner, D. M. Heyes, and S. R. Preston, Mol. Phys. **73**, 141 (1991).
[10] D. J. Evans and P. T. Cummings, Mol. Phys. **72**, 893 (1991).
[11] J. H. Irving and J. G. Kirkwood, J. Chem. Phys. **18**, 817 (1950).
[12] D. J. Evans and G. P Morriss, *Statistical Mechanics of Nonequilibrium Liquids* (Academic, London, 1990).
[13] D. L. Jolly and R. J. Bearman, Mol. Phys. **41**, 137 (1980); G. Jaccuci and I. R. McDonald, Physica A **80**, 607 (1975).
[14] M. Schoen and C. Hoheisel, Mol. Phys. **52**, 33 (1984); **52**, 1029 (1984).
[15] D. J. Evans and H. J. M. Hanley, Mol. Phys. **68**, 97 (1989).
[16] W. Loose, Phys. Rev. A **40**, 2625 (1989).
[17] D. J. Evans, R. M. Lynden Bell, ad G. P. Morriss, Mol. Phys. **67**, 207 (1989).
[18] *Transportphänomene II,* edited by R. Schäfer, Landolt-Börnstein, New Series, Group 2, Vol. XII, Pt. 5 (Springer, Berlin, 1968).
[19] W. G. Hoover (private communication).
[20] Y. Pomeau, J. Chem. Phys. **57**, 2800 (1972).
[21] H. S. Green, J. Math. Phys. **2**, 344 (1961).
[22] D. N. Zubaren, *Nonequilibrium Statistical Thermodynamics* (Plenum, New York, 1974).
[23] W. W. Wood, J. Stat. Phys. **57**, 675 (1989).
[24] P. Resibois and M. de Leener, *Classical Kinetic Theory of Fluids* (Wiley, New York, 1977).